

Submitted to Solar Physics on 6 June 2010

Sharp changes of solar wind ion flux (density) within and out of current sheets

O. Khabarova · G. Zastenker

Space Plasma Department, Space Research Institute (IKI) of Russian Academy of Sciences, 84/32 Profsoyuznaya Street, Moscow 117997, Russia

Phone: +74953331388

Fax: +74953331248

e-mail: olik3110@aol.com

Abstract Analysis of the Interball-1 spacecraft data (1995–2000) has shown that solar wind ion flux sometimes abruptly increases or decreases by more than 20% over a time period of several seconds or minutes. Typically, the amplitude of such sharp changes in the solar wind ion flux (SCIFs) is greater than $0.5 \times 10^8 \text{ cm}^{-2} \text{ s}^{-1}$. These sudden changes of the ion flux were also observed by the WIND SWE spacecraft given that the solar wind density increases and decreases with negligibly small changes in the solar wind velocity. SCIFs occur irregularly at 1 AU, when plasma flows with specific properties come to the Earth's orbit. SCIFs are usually observed in slow, turbulent solar wind with increased density and interplanetary magnetic field strength. The number of times SCIFs occur during a day is simulated using the solar wind density, magnetic field, and their standard deviations as input parameters for a period of 5 years. A correlation coefficient of ~ 0.7 is obtained between the modelled and the experimental data. It is found that SCIFs are not associated with CMEs, CIRs, or interplanetary shocks; however, 85% of the sector boundaries are surrounded by SCIFs. The properties of solar wind plasma for days with 5 or more SCIF observations are the same as those of the solar wind plasma at the sector boundaries. One possible explanation for the occurrence of SCIFs near the sector boundaries is the magnetic reconnection at the heliospheric current sheet or local current sheets. Other probable causes of SCIFs observation outside the heliospheric current sheet (inside inward or outward sectors) are turbulent processes in the slow solar wind and crossings of flux tubes' borders.

Keywords *Solar wind disturbances · Solar wind density changes · Current sheet · Sector boundaries · Small-scale structures · Plasma tubes · Magnetic reconnection · Turbulence*

Abbreviations

SCIF: sharp change of ion flux; IMF: interplanetary magnetic field; SBC: sector boundary crossing; HCS: heliospheric current sheet; CIR: corotating interaction region; CME: coronal mass ejection

1. Introduction

Experiments of the space era clearly show that solar wind properties essentially differ on different time and spatial scales (see Marsch and Liu, 1993; Velli and Grappin, 1993). The phenomena with characteristic time about hours, days and even years have been carefully studied for tens years due to regular spacecraft measurements of the interplanetary magnetic field (IMF) and plasma parameters such as the solar wind speed and the density. However, there is a whole class of poorly investigated phenomena, analyzable only on the base of rather high time-resolution data. .

Unique possibilities for studying solar wind small-scale structures appeared in 1995 when the Interball-1 spacecraft began to measure ion flux nV (where n and V are the ion density and speed respectively) using the VDP-instrument, which had a very high time resolution - no less than 1 s, (for some days it was 60 ms), (Safrankova et al. (1997)). The orbit of Interball-1 allowed the solar wind to be observed during 8 months of each year between 1995 and 2000.

One of the results of the Interball-1 mission was the observation of more than 20 000 sharp borders (characteristic width: $\sim 10^3$ – 10^4 km) of medium-scale solar wind structures (size: $\sim 10^5$ – 10^6 km). The leading and trailing sides of these structures were observed as fast and considerable changes in the solar wind dynamic pressure when the solar wind ion flux abruptly increased or decreased for more than 20% of its initial value within 10 min. Sometimes the ion flux changed several times within seconds.

Small events (amplitude: 0.5 – $1.0 \times 10^8 \text{ cm}^{-2} \text{ s}^{-1}$) were registered near the Earth's orbit, on an average, 50 times per day, and moderate and sharp ion flux changes (amplitude $\geq 2 \times 10^8 \text{ cm}^{-2} \text{ s}^{-1}$) were detected 9 times per day. List of SCIFs - Sharp Changes of Ion Flux events (when the flux increased or dropped for $> 20\%$ within 10 minutes and had an amplitude $\geq 0.5 \times 10^8 \text{ cm}^{-2} \text{ s}^{-1}$) was built for 1996–2000 by Riazantseva (see Riazantseva et al. (2002)). Explanation of the SCIFs database creation technique as well as the results of the investigations of SCIFs' fronts properties have been given in the works by a group of researchers from Solar Wind Dynamic Laboratory (IKI) since 2002 (Riazantseva et al., 2002; Dalin et al., 2002; Riazantseva et al., 2003, 2005, 2007).

Since Interball-1 did not measure the solar wind density and velocity separately, its data were compared with WIND SWE 3-s data. Riazantseva et al.

(2005, 2007) showed that all intensive changes of the ion flux with amplitude $\geq 4 \times 10^8 \text{ cm}^{-2} \text{ s}^{-1}$, detected by Interball-1, can be found from the WIND data as changes in the solar wind density. This is also true for practically all moderate SCIFs with amplitudes $\geq 2 \times 10^8 \text{ cm}^{-2} \text{ s}^{-1}$. Thus, when we refer to SCIFs below, we are primarily referring to density changes.

SCIFs are associated with neither interplanetary shock waves nor the boundaries of structures such as magnetic clouds and corotating regions (Riazantseva et al. (2005, 2007)). The basic difference between the SCIFs and the interplanetary shock waves is the absence of significant changes in the solar wind velocity (Riazantseva et al. (2005, 2007)). SCIFs mainly represent large increases or decreases in the solar wind density and resemble compressive fluctuations, which have been known since 1990 (Bruno and Carbone (2005)). However, the typical timescales for these phenomena are different (hours for compression fluctuations and minutes or even seconds for SCIFs).

Preliminary investigations have shown that SCIFs are surrounded by rather slow, but dense solar wind (Riazantseva et al. (2005a, 2007)). The other important property of SCIFs is their geoefficiency. The influence of SCIFs-caused sharp impulses of the solar wind dynamic pressure on the terrestrial magnetosphere causes significant geomagnetic field changes, local aurora borealis enhancements, and excitation of geomagnetic pulsations of different types in different geomagnetic latitudes (Borodkova et al., 2005; Parkhomov, Riazantseva, and Zastenker, 2005).

While the properties of small-scale solar wind structures, such as SCIFs, have been investigated satisfactorily, we still do not have knowledge about their origination. The following questions have yet to be answered:

1. Do SCIFs occur as a result of stochastic processes in solar wind? Alternatively, does the frequency of SCIFs' occurrence at 1 AU depend on the properties of the solar wind surrounding SCIFs?
2. Are the studied SCIFs consequences of processes on the Sun (i.e. they are related to the solar structures, keeping their form and properties while propagating from the Sun to the Earth)? Alternatively, do SCIFs occur directly in solar wind plasma as the result of the processes, taking place in space (i.e. turbulence or instability in solar wind plasma)?
3. What is the lifespan of SCIFs?

For the best understanding of the processes observed in near-Earth space, we must investigate the properties of medium- and large-scale SCIFs. Here, we study the first question in detail and make assumptions on the nature of SCIFs observed at 1 AU. The analysis of solar wind plasma conditions related to SCIFs includes a case study, statistical analysis of experimental data, and modelling.

2. Sharp density changes occurring at 1 AU and the corresponding solar wind conditions

2.1. A CASE STUDY

A typical case of a sharp solar wind density or ion flux change near 1 AU is shown in Figure 1. Figure 1a shows the SCIFs on 26 April 1998, which were measured by both the WIND 3DP (time resolution: 3 s) and Interball-1 VDP instruments (time resolution: 1 s), with a time delay of ~ 1.5 h, as spacecraft were at ~ 200 Re. For illustration purposes, the data from WIND is time shifted to match the Interball-1 data in Figure 1a. We use arrows to indicate the start times of SCIFs (intense increases or decreases in ion flux with amplitudes $\geq 2 \times 10^8 \text{ cm}^{-2} \text{ s}^{-1}$) on the Interball-1 ion flux curve.

Despite a slight transformation along the propagation path of the SCIFs-containing stream, it is easy to observe similar sharp changes in the solar wind density (measured by WIND 3DP) and ion flux (measured by Interball-1). More examples of SCIFs measured by Interball-1 and their corresponding density changes (measured by the WIND and IMP8 spacecraft) can be found in papers by Riazantseva et al. (2002, 2003, 2005) and Dalin et al. (2002b).

Figure 1a shows that small-scale boundaries of medium-scale flows are rather stable and do not disappear during solar wind propagation at ~ 200 Re. Thus, SCIFs are not a result of small-scale instability (in the opposite case their life-time would be significantly shorter) and they are not specific features of the Earth magnetosphere foreshock region (as otherwise they would be observed only by Interball-1). Moreover, according to Dalin et al. (2002), there are examples of SCIFs that remained stable for distances up to 0.6 AU. Therefore, either SCIFs originate on the Sun with their consequent transference by solar wind streams, or they are a result of some large-scale processes in space.

The OMNI2 time series of hourly averaged solar wind parameters are given in Figures 1b, c for the entire day of 26 April 1998. Vertical boxes in Figure 1b show the number of SCIFs per hour with amplitudes $\geq 0.5 \times 10^8 \text{ cm}^{-2} \text{ s}^{-1}$. If we analyse the properties of the stream that carried SCIFs to the Earth's orbit, we see that the substantial growth in the number of SCIFs' per hour is accompanied by a significant growth in the solar wind density and its standard deviation (Figure 1b), while other key background parameters remain stable (Figure 1c).

Visual analysis of Interball-1 and OMNI2 data has shown that most days with high SCIFs number are characterized by plasma conditions similar to those represented in Figure 1. (We will confirm this statement using statistical analysis below.) Thus, SCIFs are not a result of random processes in space plasma, but are structures related to streams with specific conditions.

One confirmation of this idea is SCIFs' grouping: days with high number of SCIFs alternate with the days without SCIFs or with their very small number. Nine events per day (as was mentioned in the Introduction) is an averaged rate of the occurrence of SCIFs at the Earth's orbit. It does not reflect the actual SCIFs observation frequency; therefore, we have to carry out a more careful investigation of SCIFs' temporal distribution.

2.2. FEATURES OF SCIFs TEMPORAL DISTRIBUTION

In this section, we analyse the statistical properties of 5 300 SCIFs, with amplitudes greater than $2 \times 10^8 \text{ cm}^{-2} \text{ s}^{-1}$, observed during 427 of the 673 days when Interball-1 was in the solar wind (for time period from 28 February 1996 to 21 September 2000). To ensure clean results, all days where Interball-1 passed through the foreshock region were removed from consideration.

The time distribution of the number of SCIFs per day ($N_{\text{SCIF/day}}$) is shown in Figure 2. The horizontal axis represents the daily number of SCIFs, and the vertical axis represents the class frequency in percent of the entire body of SCIFs. This histogram is drawn as follows: we take the number of SCIFs per day ($N_{\text{SCIF/day}}$) and multiple it by the number of days when the given $N_{\text{SCIF/day}}$ is observed. For example, 4 SCIFs per day were observed by Interball-1 34 times during the 1996–2000 observations. Hence, whole number of SCIFs, observed with such frequency is 136. Then, we divide the x-axis into several spans such as

$0 \leq N_{\text{SCIF/day}} < 2$ and $2 \leq N_{\text{SCIF/day}} < 4$ and calculate the number of SCIFs occurring in the specific range of $N_{\text{SCIF/day}}$ values.

The obtained distribution is significantly shifted from the Gaussian distribution: about 50% of the total number of events were observed from 17 to 64 times per day. This demonstrates the grouping effect: on some days, SCIFs are observed sequentially in a pulse packet that probably contains the small-scale boundaries of some medium- or large-scale solar wind structures.

The results of this statistical analysis allow us to assume that it is possible to evaluate $N_{\text{SCIF/day}}$ as a function of parameters of the ambient solar wind. We will seek the most characteristic changes of key solar wind parameters during the periods with large numbers of SCIFs and build a modelling function on the basis of the parameters best correlated with $N_{\text{SCIF/day}}$.

2.3. BEHAVIOUR OF SOLAR WIND PARAMETERS DURING PERIODS OF SCIFs PACKETS' OCCURENCE AT 1 AU

2.3.1 Analysis of histograms

The characteristics of the SCIFs-containing streams will be analysed through statistical properties of days with high SCIFs number. We consider a day to be a 'SCIF pulse-packet day' if the number of SCIFs exceeds five that day ($N_{\text{SCIF/day}} \geq 5$). There were 264 days (containing 4 951 SCIFs) that satisfied this condition. This means that 93% of SCIFs were observed during 'SCIFs pulse-packet days' (which make up 62% of the total number of days); therefore, the grouping effect is strongly expressed.

Analysis of the solar wind plasma properties for those days shows that SCIFs-containing large and medium-scale structures can be characterised by enhanced solar wind density n (Figure 3a), slightly increased average IMF magnitude $|B|$ (Figure 3b), and an increased standard deviation of both density and the IMF (Figures 3c and d). The white boxes in Figure 3 represent the distribution of parameters for the days with high SCIFs number for 1996–2000, and the black boxes show the distribution of the same parameters for the same time range according to WIND SWE daily data. The standard deviations obtained from the mean in Figures 3c and 3d are calculated using the hourly WIND SWE data. In all cases, there is a shift of the white histograms to the right, relative the black ones,

especially for the density and its standard deviation. The statistical characteristics of the histograms are listed in Table 1, where the distributions for the entire time period of measurements and for days when $N_{\text{SCIF/day}} \geq 5$ are marked as ‘all’ and ‘scif’, respectively.

According to the t-test, the difference between all pairs of ‘all-scif’ variables is statistically significant (the t-test meets the conventional significance level less than 0.05 ($p < 10^{-6}$)). This means that the histogram shifts in Figure 3 were not obtained by chance.

It is interesting to note that the skewness of the ‘scif’ histograms are lower than the corresponding ones for ‘all’ data (see Table 1). Skewness measures the deviation of the distribution from symmetry. If the skewness is clearly different from 0, then the analyzed distribution is asymmetrical, while normal distributions are perfectly symmetrical. The asymmetry of the solar wind parameters’ distributions is an evidence of some structuring of the solar wind plasma. In our case, the closeness of ‘scif’ distributions to the Gaussian could mean that stochastic processes in SCIFs-containing plasma occur more often than usual or that such plasma streams originate far from the solar wind source.

There is one more confirmation that SCIFs are observed in the turbulent solar wind. We compared the IMF variability in the ULF frequency band (ULF wave index) for days with high SCIFs number to the variability over the entire time period of observations (Figure 4). The ULF index is a 1-h resolution index, which characterises the turbulence level of the solar wind magnetic field in the ULF range (Romanova et al., 2007) and is calculated from 1-min three components of the IMF (measured by WIND or ACE). The higher the ULF-index value, the higher is the IMF disturbance level in the 1–10 mHz frequency range.

The black histogram shown in Figure 4 represents the distribution of the ULF index for 1996–2000, and the white histogram shows the distribution of the ULF index for the days when SCIFs have been observed by Interball-1 greater than or equal to five times per day. The shift of the white histogram to the right denotes a high level of magnetic field turbulence in SCIFs-containing solar wind streams.

It is interesting that difference between the histograms in Figures 3-4 remains statistically significant for the amplitudes lower than $2 \times 10^8 \text{ cm}^{-2} \text{ s}^{-1}$, but the higher is SCIFs’ amplitude, the significantly are characteristic shifts. Similar properties have recently been found by Riazantseva et al. (2005a, 2007) as a result of the

analysis of solar wind parameters histograms in a range of 30 min around the moment of SCIF observation. This demonstrates the existence of medium- or large-scale dense, turbulent regions, carrying SCIFs to 1 AU.

2.3.2. *A superposed epoch analysis*

A method of superposed epoch (compositing analysis) is often applied to time series in solar-terrestrial physics for the analysis of conditions accompanying repeated events (see, for example, Lavraud et al., 2005). The main concept of the superposed epoch analysis method is that data averaging purifies the useful signal and suppresses the noise. A picture in the absence of the effect usually looks like a stochastic curve (or even as a straight line), which does not fall outside the limits of 95% confidence interval. On the contrary, statistically significant results are obtained when the extreme points with their standard deviations are beyond the 95% confidence interval, plotted on each side of the mean value line.

Figure 5 shows the behaviour of the main plasma parameters averaged over the days with high SCIFs number. Zero-day corresponds to the day of observation with 5 or more SCIFs (264 cases). We have put all the statistical information into Table 2 to clearly show the effect.

The increases in density, interplanetary magnetic field, and their standard deviations for days of high SCIFs number are confirmed by superposed epoch analysis results. Figures 5a, b show that a significant increase in the parameters is observed in the two-day range around zero-day.

The behaviour of the geomagnetic K_p -index is an indirect confirmation of SCIFs' (or the SCIFs-containing stream's) geoefficiency. The K_p -index increases on the day of the SCIFs-packet interaction with terrestrial magnetosphere (see Figure 5c). The effect lasts up to two days. The interesting fact is that the solar wind speed decreases before zero-day and increases symmetrically after that, though the changes are rather small.

2.4. LINEAR CORRELATION ANALYSIS

An analysis of solar wind key parameters' correlation with frequency of SCIFs occurrence at 1 AU was performed. It was found that the number of SCIFs per day does not correlate with the OMNI2 time series of the daily averaged solar wind speed V , the electric field ($-\mathbf{V} \times \mathbf{Bz}$), beta parameter, or the Alfven Much

number, and it poorly correlates with the standard deviation of V . The correlation coefficients between $N_{\text{SCIF/day}}$ and these parameters do not exceed 0.22, as shown in Table 3.

We have removed the hours with SCIFs from the **sigma n** time series to avoid SCIFs' possibly increasing the standard deviation of the density and to ensure the absence of artefacts in our statistical analysis and modelling. Results of the correlation analysis for SCIFs number per day and solar wind parameters, shown in Figure 3, are summarized in Table 4. The $N_{\text{SCIF/day}}$ time series show behaviour similar to that of density, the IMF averaged magnitude, and their standard deviations. The correlation coefficients listed in Table 4 are up to 0.5.

Thus, if we want to find a modelling parameter, characterising the frequency of the occurrence of SCIFs at 1 AU as a function of some solar wind parameters, we have to focus on the solar wind density, the interplanetary magnetic field, and their variabilities.

3. Modelling

A composite function method has been used for modelling. This method assumes that if the parameters, taken separately, correlate with a variable just moderately, their optimal combination could give higher correlation with this variable. After the correlation analysis, the positive correlating parameters are placed in the numerator and the negative ones are placed in the denominator. An expert evaluation, in combination with computer coefficients adjustment, gives the best chance to find the optimal parameters for simulating the variable. The method is analogous to the neural network and demands an extremely good knowledge of simulated processes from an investigator.

The result of seeking various modelling functions for finding the most effective fitting parameter $P_{\text{SCIF/day}}$ to simulate the number of SCIFs per day $N_{\text{SCIF/day}}$ includes plasma and magnetic parameters. This is expressed as follows:

$$P_{\text{SCIF/day}} = -2.398 + 0.0267 \times (\text{sigma}n + 4 \times n) \times (3 \times \text{sigma}B + |B|) \quad (1),$$

where n is the solar wind density (cm^{-3}); $|B|$ is the IMF averaged magnitude (nT); $\text{sigma}n$ is the standard deviation of the solar wind density (cm^{-3}), with the hours with SCIFs removed to avoid artefacts; and $\text{sigma}B$ is the standard deviation of interplanetary magnetic field averaged magnitude (nT).

As we can see from (1), there are two multipliers, which represent density and the IMF input. Synchronous increasing of density and IMF together with their variations provides the best conditions for SCIFs origination or propagation. As it will be shown below, such solar wind conditions exist around current sheets (sector boundaries).

An example of the modelling realisation for 2000 is shown in Figure 6, where the experimentally observed frequency of SCIFs' observation by Interball-1 is shown in comparison with the fitting parameter $P_{SCIF/day}$ (Figure 6a), its multipliers $\sigma n + 4 \times n$ (Figure 6b), and $3 \times \sigma |B| + |B|$ (Figure 6c). A rather good match of the $P_{SCIF/day}$ parameter with the observed data is found.

It is remarkable that the correlation coefficients between the experimentally observed number of SCIFs per day and all the parameters, included in $P_{SCIF/day}$, are no more than 0.5 (see Table 4 and Figures 6b and c). At the same time, the correlation coefficient between $N_{SCIF/day}$ and the revealed modelling function $P_{SCIF/day}$ is 0.7. All these correlation coefficients are calculated for entire period of observations (1996–2000).

$P_{SCIF/day}$ and $N_{SCIF/day}$ have identical means and close standard deviations (8.8 for $P_{SCIF/day}$ and 13.0 for $N_{SCIF/day}$). Therefore, from a statistical point of view, we have very similar data rows, and they do not coincide by chance.

These facts confirm the success of the simulation and give us possibility to conclude that the IMF, solar wind density and their variabilities, bring the cumulative contribution to stabilisation and propagation (or even occurrence) of SCIFs.

4. Current sheets and sharp changes of solar wind density and ion flux

Now, it is reasonable to consider the physical sense of the discussed phenomenon. Rather important facts can be found from comparing the time when the SCIFs were measured with the arrival of such structures as magnetic clouds (MCs), corotating interaction regions (CIRs), and sector boundaries. The dates of the beginning and end of MCs and CIRs passages, as well as the sector boundary crossings (SBCs) for 1996–2000, were taken from an open source catalogue (ISTP Solar Wind Catalogue of Candidate Events). A SCIF event was considered to be associated with one of these large-scale structures if it occurred within a

time interval starting a day before the corresponding structure's arrival at 1 AU and ending a day after its termination.

It was found that SCIFs are practically not associated with the first two structures, i.e. no more than 2% of them are located within (or around) MCs or CIRs (Khabarova and Zastenker (2008)). On the other hand, an overwhelming majority of sector boundaries in 1996–2000 (85%) were surrounded by SCIFs.

The analysis has shown no increase or decrease in the SCIFs' amplitude within the sector boundary areas. We simply observe a stable increase in the SCIFs' number in the sector boundary's vicinity. Analysis shows that 38% of all cases of SCIF observations having between 9 and 64 events per day correspond to the current sheet crossings. Meanwhile, 64 SCIFs per day are observed near sector boundaries only in 25% of the cases.

It is remarkable that the features of solar wind plasma for 141 non-SBC-related days with high SCIFs number, analysed in the sections 2.3.1 and 2.3.2, are the same as those for 123 SBC-related ones. Therefore, although we cannot explain the occurrence of all SCIFs at the Earth's orbit by processes in only the current sheets, analysis of solar wind conditions at currents sheets and around them probably could give us a key for understanding the nature of the entire body of events.

4.1 SOLAR WIND PARAMETERS' BEHAVIOUR AT CURRENT SHEETS

An increase in the ion flux near sector boundaries was first mentioned in 1984 by Briggs and Armstrong (1984); however, the nature of this phenomenon has not practically been investigated after them. Let us look closely at the plasma properties in the sector boundary vicinities and compare them with the typical plasma characteristics where SCIFs were observed.

The commonly accepted picture describes sector boundaries as a result of intersection of the heliospheric current sheet (HCS), which is formed by an extension of the main solar neutral line (the heliomagnetic equator). The HCS, discovered by Wilcox and Ness (1965), divides the heliosphere into the areas of opposite IMF direction - sectors (Svalgaard et al. (1975)). It is known that sector boundary crossings (SBCs) are accompanied by an increase in the plasma density

and a decrease in the solar wind speed near zero-line (Schwenn, 1990; Smith, 2001; Crooker et al., 2004; Blanco, 2006).

Theoretically, the sector boundary must correspond with the HCS; however, in reality, this view is simplified and only appropriate for educational purposes. Close investigations show that there are problems that arise with identification of the HCS on the basis of the SBC data. First, the main solar zero-line does not always coincide with sector boundaries owing to the magnetic field complications that arise on the way from the Sun to the Earth, as shown by Crooker et al. (2004). Loop structures can entangle the IMF and form local current sheets with field reversals, which are not true the HCS' sector boundaries. The local zero lines between groups of sunspots, reaching 1 AU, can also be identifiable as current sheets (or sector boundaries crossing).

Another problem is that the HCS and even the local current sheets are not truly sheets. Owing to their complex internal structure or undulating movement, a crossing of these large-scale structures at 1 AU can last for several hours or even days. In the result spacecraft meets several sector boundaries for one current sheet (Blanco et al., 2006). This fact complicates the identification of sector boundary crossings and leads to contradictory results, as investigators sometimes consider the heliospheric current sheet to be a very thin layer and believe that its crossing takes no more than several minutes.

Figure 7 shows the distribution of SBC durations after the ISTP Solar Wind Catalogue of Candidate Events for 1994–2000. The magnetic field's reversal process, as illustrated by figure 7, mainly takes no more than one day (149 cases). Two-day length SBCs were observed only 49 times, with very few of the cases corresponding to a 3–8 day long unstable IMF direction.

The methods of sector boundaries identification are slightly different. SBCs are mainly determined by changes in the interplanetary magnetic field longitude angle ϕ_B (IMF azimuth $\phi-B$) due to changes in the horizontal B_x and B_y IMF components. Sometimes investigators simply look at the IMF B_x component's changing sign, and sometimes they additionally use suprathermal electron data for SBC dates list creating (see Crooker et al. (2004)). Geomagnetic field data are also used for this purpose, especially for times prior to the space era (Svalgaard, (1975)). All of these may lead to inconsistent results and misunderstandings in the analysis of heliospheric current sheet properties.

Consequently, there are several poorly coincided lists of SBC dates in the open Internet access (see, for example, ISTP Solar Wind Catalogue <http://www-spof.gsfc.nasa.gov/scripts/sw-cat/grep-ls/sw-cat-categories.html>; The Wilcox Solar Observatory List <http://wso.stanford.edu/SB/SB.html>, and OMNIweb list http://omniweb.gsfc.nasa.gov/html/polarity/polarity_tab.html) and some ‘private’ lists, made by several investigators for their own scientific aims (see, for example, Leif Svalgaard’s List at <http://www.leif.org/research>).

Analysis of the solar wind parameters’ behaviour at the HCS and local current sheets has been performed to compare the current sheets’ key properties with features of SCIFs’ packets occurrence (see Figures 5 and 8). To obtain the best statistics and avoid mistakes, we used a method of superposed epoch for two lists of SBCs: the list by Leif Svalgaard, containing 1 300 events for the period of available OMNI2 data from January 1964 to April 2010 (Figures 8a–c) and the ISTP Solar Wind Catalogue Candidate Events for the abovementioned 149 one-day sector boundaries crossings between 1994 and 2000 (see Figures 8a’–c’).

The typical solar wind parameters’ profiles over the day of sector boundary crossing are shown in Figure 8, and their statistical properties are listed in Table 5 (left panel of Figure 8) and Table 6 (right panel of Figure 8).

The IMF strength growths on the SBC days, as we can see from Figures 8a, a’. But from theoretical point of view the average IMF module must drop at the moment of sector boundaries crossing. There is no a contradiction in this. Precise data show that all of the IMF components drop at the current sheet for very short time (several minutes) and that the current sheet is surrounded by regions of increased IMF. Therefore, the IMF increase at a zero-day is a result of 24-h averaging.

The well-known growth of the solar wind density over the heliospheric current sheet is observed in a wide time range - from one day before the SBC to two days after (Figure 8b,b’).

The increased variabilities of density and the IMF strength around sector boundaries paint a complicated picture of instabilities, which develop at the current sheets. As a result, the current sheets’ plasma tends to be highly disturbed.

Growth of geomagnetic activity at the heliospheric current sheet crossing, represented by Kp-index (see Figure 8c,c’), is an interesting feature, which has

been investigated for many years (see the pioneer works by Hirshberg and Colburn, 1973; Hakamada, 1980).

The reducing of Kp-index one-two days before sector boundary crossing is not a well-known effect, in spite of its discovery in 1973 by Leif Svalgaard (Svalgaard, 1973). This phenomenon was recently ‘refreshed’ by Watari and Watanabe (2006), who investigated the behaviour of the Kp-index around the HCS in dependence on solar cycle.

The solar wind speed decrease before the sector boundaries and its subsequent increase is a rarely discussed phenomenon, although this effect also was mentioned in the pioneer works by Svalgaard (1973, 1975). Usually, the speed is considered to be lower around the HCS (Borrini et al., 1981). The nature of the non-symmetric profiles of Kp and the solar wind speed over current sheets has been investigated in only a few works. Neugebauer et al. (2004) mentioned in their case-study investigation the decreasing speed of the solar wind before the observed sector boundaries and after them. Referring to von Steiger et al. (2000), the authors believe that it is possible to explain this phenomenon by the various natures of streams before and after the HCS. Lacombe et al. (2000) suppose that the solar wind speed depression before the HCS is a feature of high-pressure solar wind, which is a result of the dynamical stream interactions.

The interesting and intriguing fact is almost full identity of the parameters’ behaviour in Figures 8 and 5. This means that either HCS typical conditions are ideally suited for keeping/transition of SCIFs or the HCS is a direct place where they originate.

4.2 THE PHYSICAL NATURE OF THE OBSERVED SHARP DENSITY CHANGES WITHIN CURRENT SHEETS AND IN SLOW SOLAR WIND

We showed in 2.3 that SCIFs are observed in dense and turbulent regions of the solar wind. We also found out in previous studies that the speed of the solar wind surrounding SCIFs is lower than usual (Riazantseva et al. (2007)). The increased turbulence in dense, slow plasma leading to large-scale instabilities at the HCS or the local current sheets could be a cause of SCIFs occurrence at 1 AU. Properties of near-HCS zone of raised turbulence, containing discontinuities, are still insufficiently investigated (Crooker et al., 2004; Blanco et al., 2006; Marsch, 2006). Roberts, Keiter, and Goldstein (2005) noticed that many dynamic

processes go on permanently inside the HCS, and its structure becomes more and more turbulent and complex with heliocentric distance.

Any large-scale instability near the IMF nil-line inside the HCS can be a cause of magnetic reconnection. The works of many authors confirm this idea, obvious from the general reasons (for example, Murphy et al., 1993; Gosling et al., 2006; Phan, Gosling, and Davis, 2009).

The heliospheric current sheet not only extends during the process of distribution from the Sun, but also is enriched by products of repeated reconnections at the zero-line. Arising waves, discontinuities, and soliton-like structures are observed by many spacecraft both at the sector boundaries, and in their near vicinity. Probably, we face here beamlet-structures (double ion beams), which sometimes are observed in the vicinity of sector boundaries. Hammond et al. (1995) described them in their work and postulated that these beams are result of magnetic reconnection.

Since the solar wind properties for the days with SBC-related SCIFs and non-SBC-related ones are the same, the question now arises as to whether SCIFs', which are observed far from sector boundaries, and the HCS-associated SCIFs, have the same nature?

Neugebauer et al. (2004) noticed that the non-HCS slow solar wind includes a lot of small-scale structures, such as discontinuities, magnetic holes, and low-entropy structures. These structures are usually associated with the slow solar wind around the HCS. Therefore, turbulent processes in the slow solar wind could be a key cause of SCIFs observed in the non-HSC solar wind.

It is possible to suppose that the observation of the non-HCS part of SCIFs can be explained by the presence of flux tubes in the solar wind. The concept of separated thin plasma tubes (or spaghetti-like structures) existing in the solar wind plasma has been put forward repeatedly for more than 40 years (see the review by Wang and Sheeley, 1990; Hollweg, 1972, 1986; Wang, 1993; Li, 2003) since Parker (1963) first suggested it. Recently, Borovsky (2008) presented a rather convincing evidence for the existence of plasma tubes and came to the important conclusion that the tubes are larger in slow wind than in fast wind. It has been estimated that the median size of the flux tubes at 1 AU is 4.4×10^5 km.

SCIFs could be a sign of such tubes' crossings, as SCIFs in the SCIF-packet are usually observed with a time lapse of several minutes, sometimes hours (see

an example in Figure 1a, where SCIFs are observed more frequently than 1 h from 8 h to 15 h and more rarely from 17h to 21h). This corresponds a distance of about 10^5 – 10^6 km (Riazantseva et al., 2002; Dalin et al., 2002; Riazantseva et al., 2003). Therefore, the characteristic size of the structures with sharp borders (detected as SCIFs) coincides with the estimated sizes of the flux tubes.

Qin and Li (2008) recently constructed a model of the solar wind turbulence, which consists of independently moving flux-tube structures (cells). They believe that local current sheets (not the HCS) are possibly the boundaries of such individual flux tubes.

Thus, both magnetic reconnection and turbulence are possible causes of non-HCS SCIFs in the slow solar wind. Another possibility is that such SCIFs are the result of reconnection directly on the Sun in the large coronal loops, which form slow solar wind streams (von Steiger, 2000).

5. Conclusions

The sharp change of the solar wind ion flux - SCIF is a very fast and abrupt process. SCIFs were found during the analysis of the Interball-1 spacecraft high-resolution data (1995–2000). They take from seconds to minutes to pass spacecraft, and the solar wind ion flux can increase/decrease several times during these passages. After comparing the Interball-1 SCIF database with WIND SWE data, it was found that SCIFs are primarily changes of density.

SCIFs are not a feature of foreshock area ahead the Earth magnetosphere. They are rather long-living structures, sometimes they are traced at the distance up to 0.6 AU. SCIFs are not a result of local instabilities, but they are related to some large-scale processes in solar wind (or, possibly, on the Sun). SCIFs are not associated with interplanetary shocks, CIRs or CMEs, but frequently observed near the sector boundaries.

On the basis of the current investigation, we can conclude that

1. SCIFs with amplitudes greater than $2 \times 10^8 \text{ cm}^{-2} \text{ s}^{-1}$ usually come to the Earth's orbit in a pulse packet, with up to 128 events per day (we define that a pulse-packet is observed when SCIFs number per day exceeds five). 93% of SCIFs measured by Interball-1 belonged to pulse packets, which were observed during 62% of all days. The grouping effect is proved both by case study and statistical

analysis. This can be a sign of the episodic occurrence of solar wind streams containing discontinuities at 1 AU.

2. Analysis of the solar wind properties of SCIFs-containing streams shows that SCIFs are observed in dense, turbulent solar wind, with slightly increased values of the IMF strength. For example, a superposed epoch analysis shows that the standard deviations of density and IMF are correspondingly 1.9 and 1.6 times larger in the days with high SCIFs number than in the days with no SCIFs. The density increases by a factor of 1.4, and the IMF magnitude increases by a factor of 1.2 during the days where SCIFs pulse-packets are observed. In combination with the results of previous work that shows that SCIFs mainly occur in slow solar wind, this gives us possibility to conclude that SCIFs hardly related to active solar processes such as solar flares and coronal mass ejections. They are also not generated in (or around) dense solar wind regions like CIRs, but they could be a result of turbulence in slow solar wind or in the solar corona.

3. The number of SCIFs per day can be successfully simulated by a combination of the key solar wind parameters comprising the solar wind density, interplanetary magnetic field, and their variabilities. A correlation coefficient between the revealed modelling parameter and the observed number of SCIF's per day is 0.7. This means that the occurrence of SCIFs at the Earth's orbit is not a random process, but a result of specific plasma conditions. As we can see from the previous conclusion, SCIFs-containing streams have properties that are significantly different from the properties of the ambient solar wind. Simulations show that SCIFs most frequently occur under condition of coincidence of the solar wind density and IMF strength increasing (as well as growth of their variability). At 1 AU, such plasma properties are mainly observed at sector boundaries in the solar wind.

4. SCIFs are associated with sector boundaries crossings. 85% of all tested sector boundaries were surrounded by SCIFs. The conditions favourable for origination and propagation of SCIFs exist in the ± 1 day vicinity of the heliospheric current sheet (HCS) and local current sheets.

5. A considerable percentage of SCIFs (60% from the total) are observed far from the sector boundaries (inside outward or inward sectors) in the slow solar wind when the HCS-like conditions exist. On the basis of the obtained results, we

hypothesize that the HCS-like conditions play a key role in formation of the discussed ion flux (density) changes.

As a typical time span between SCIFs is several (or tens) minutes and the SCIFs-passage time is no more than 10 min, we can consider SCIFs as the borders (with characteristic size $\sim 10^3$ – 10^4 km) of some plasma structures whose width is $\sim 10^5$ – 10^6 km. These plasma structures have specific properties and represent solar wind streams, observed both around sector boundaries and inside sectors.

We suppose that the nature of SBC-related SCIFs could be investigated through analysis of the reconnection process both at the HCS and local current sheets (which are separators of sunspot groups of the opposite sign), as discontinuities around HCS mainly occur as the result of turbulence and repeating magnetic reconnection at X-line.

SCIFs, not related to the SBC, could indicate crossings of flux tubes in the solar wind. Such tubes are supposed to exist in relatively slow solar wind, undisturbed by fast streams like CME. It is remarkable that their median size is estimated as $\sim 10^5$ – 10^6 km, which coincides with size of the structures containing SCIF.

The other possible origin mechanism for SCIFs is turbulence. Slow solar wind is more turbulent than fast. As a result, numerous discontinuities are a typical feature of slow solar wind.

All the mechanisms listed above will be the subjects of future testing and investigations. The analysis of distanced spacecraft data could be particularly useful as it could help to draw the picture of SCIFs origin and propagation in the solar wind, and give us some answers to key questions about their nature.

Acknowledgements The one-second plasma data are obtained in the result of the Interball mission (see <http://www.iki.rssi.ru/interball>). WIND 3DP solar wind data with 3 second resolution are from web-site of Goddard Space Flight Center: <http://cdaweb.gsfc.nasa.gov>, and OMNI2 data are taken from the official OMNIweb site: <http://omniweb.gsfc.nasa.gov/ow.html>. The detailed list of sector boundaries crossings (ISTP Solar Wind Catalogue of Candidate Events) is presented on <http://www-spf.gsfc.nasa.gov/scripts/sw-cat/grep-ls/SBC.html>. SBC List by Leif Svalgaard was taken from his official web-page: <http://www.leif.org/research/sblist.txt>. Data, articles and the detailed description of ULF-index calculation technique can be found on ftp://space.augsburg.edu/macacs/ULF_Index. The authors wish to thank Dr. Elena Driver (St.Mary's University College, London) for her linguistic remarks. This research was supported by RFBR's grants 10-02-00277-a, 08-02-92212-a, and partially by 10-02-01063-a grant.

References

- Blanco, J.J. , Rodriguez-Pacheco, J., Hidalgo, M.A., and Sequeiros, J.: 2006, Analysis of the heliospheric current sheet fine structure: Single or multiple current sheets. *J. Atm. Sol.-Ter. Phys.* **68**, 2173–2181.
- Borodkova, N.L., Zastenker, G.N., Riazantseva, M.O., and Richardson, J.D: 2005, Large and sharp solar wind dynamic pressure variations as a source of geomagnetic field disturbances in the outer magnetosphere (at the geosynchronous orbits. *Planet. Space Sci.* **53**, 25-32.
- Borovsky, J. E.: 2008, Flux tube texture of the solar wind: Strands of the magnetic carpet at 1 AU. *J. Geophys. Res.* **113**, A08110.
- Borrini, G., Gosling, J., Bame, S., Feldman, W., and Wilcox, J.: 1981, Solar wind helium and hydrogen structure near the heliospheric current sheet: a signal of coronal streamers at 1 AU. *J. Geophys. Res.* **86**, 4565-4573.
- Briggs, P. R., and Armstrong, T. P.: 1984, Observations of interplanetary energetic ion enhancements near magnetic sector boundaries. *Geophys. Res. Lett.* **11**, 27–30.
- Bruno, R., and Carbone, V.: 2005, The solar wind as a turbulence laboratory. *Living Rev. Solar Phys.* **2**, <http://www.livingreviews.org/lrsp-2005-4>.
- Crooker, N. U., Huang, C.-L., Lamassa, S. M., Larson, D. E., Kahler, S. W., and Spence, H. E.: 2004, Heliospheric plasma sheets. *J. Geophys. Res.* **109**, A03107.
- Dalin, P. A., Zastenker, G. N., Nozdrachev, M. N., and Veselovsky, I. S.: 2002a, Properties of large and sharp impulses in the solar wind. *Int. Journ. Geom. Aeron.* **3**, 51-56.
- Dalin, P. A., Zastenker, G. N., Paularena, K. I., and Richardson, J. D.: 2002b, A survey of large, rapid solar wind dynamic pressure changes observed by Interball-1 and IMP 8. *Annales Geophysicae*, **20**, 293–299.
- Gosling, J. T., McComas, D. J., Skoug, R. M., and Smith, C. W.: 2006, Magnetic Reconnection at the Heliospheric Current Sheet and the Formation of Closed Magnetic Field Lines in the Solar Wind. *Geophys. Res. Lett.* **33**, L17102.
- Hakamada, K.: 1980, Geomagnetic activity at the time of heliospheric current sheet crossings, *Geophys. Res. Lett.* **7**, 653–656.
- Hammond, C. M.; Feldman, W. C.; Phillips, J. L.; Goldstein, B. E.; Balogh, A.: 1995, Solar wind double ions beams and the heliospheric current sheet. *J. Geophys. Res.* **100**, 7881-7889.

- Hirshberg, J. and Colburn, D. S.: 1973, Geomagnetic activity at sector boundaries, *J. Geophys. Res.* **78**, 3952–3957.
- Hollweg, J.V.:1972, Supergranulation-driven Alfvén waves in the solar chromosphere, and related phenomena. *Cosmic Electrodynamics* **2**, 423-444.
- Hollweg, J.V.: 1986, Transition region, corona, and solar wind in coronal holes. *J. Geophys. Res.* **91**, 4111-4125.
- Khabarova, O.V. and Zastenker, G.N.: 2008, Sharp and sizeable changes of solar wind ion flux as a feature of dense non-CIR turbulent regions, *Geoph. Res. Abstracts*, 10, EGU2008-A-09908.
- Lacombe, C., Salem, C., Mangeney, A., Steinberg, J.-L., Macsimovic, M., and Bosqued, J.M.: 2000, Latitudinal distribution of the solar wind properties in the low- and high-pressure regimes: Wind observations. *Ann.Geoph.* **18**, 852-865.
- Lavraud, B., Denton, M. H., Thomsen, M. F., Borovsky, J. E., and Friedel, R. H.W.: 2005, Superposed epoch analysis of dense plasma access to geosynchronous orbit. *Ann. Geophys.* **23**, 2519–2529.
- Li, X.: 2003, Transition region, coronal heating and the fast solar wind. *Astron. and Astrophys.* **406**, 345–356.
- Marsch, E. and Liu, S.: 1993, Structure functions and intermittency of velocity fluctuations in the inner solar wind. *Ann. Geophys.* **11**, 227-238.
- Marsch, E.: 2006, Kinetic Physics of the Solar Corona and Solar Wind. *Living Rev. Solar Phys.* **3**, 1, <http://www.livingreviews.org/lrsp-2006-1> .
- Murphy, N., Smith, E.J., Burton, M.E., Winterhalter, D. and McComas, D.J.: 1993, Energetic ion beams near the heliospheric current sheet: possible evidence for reconnection. *Jet Propulsion Lab.(NASA) Technical Report*, <http://trs-new.jpl.nasa.gov/dspace/bitstream/2014/35959/1/93-1689.pdf> .
- Neugebauer, M., Liewer, P. C., Goldstein, B. E., Zhou, X., Steinberg, J. T.: 2004, Solar wind stream interaction regions without sector boundaries. *J. Geophys. Res.* **109**, A10102.
- Parker, E.N.: 1963, *Interplanetary Dynamical Processes*, New York, Interscience.
- Parkhomov, V.A., Riazantseva, M.O., and Zastenker, G.N.: 2005, Local amplification of auroral electrojet as response to sharp solar wind dynamic pressure change on June 26, 1998. *Planet. Space Sci.* **53**, 265-274.
- Phan, T. D., Gosling, J. T., and Davis, M. S.: 2009, Prevalence of extended reconnection X-lines in the solar wind at 1 AU. *Geophys. Res. Lett.* **36**, L09108.

- Qin G. and Li G.: 2008, Effect of flux tubes in the solar wind on the diffusion of energetic particles. *Astrophys. J.* **682**, L129–L132.
- Riazantseva, M.O., Dalin, P.A., and Zastenker, G.N.: 2002, Statistical analysis of fast and large impulses of solar wind ion flux (density) as measured by Interball-1. *Soln.-zemn. fizika* **2**, 89-92.
- Riazantseva, M. O., Dalin, P. A., Zastenker, G. N., Parhomov, V. A., Eselevich, V. G., Eselevich, M. V., and Richardson, J.: 2003a, Properties of Sharp and Large Changes in the Solar Wind Ion Flux (Density). *Cosmic Res.* **41**, 395–404.
- Riazantseva, M.O., Dalin, P.A., Zastenker, G.N., and Richardson, J.: 2003b, Orientation of sharp fronts in the solar wind plasma, *Cosmic Res.* **41**, 405–416.
- Riazantseva, M.O., Khabarova, O.V., and Zastenker, G.N.: 2005a, Sharp boundaries of solar wind plasma structures and an analysis of their pressure balance. *Cosmic Res.* **43**, 157-164.
- Riazantseva, M.O, Zastenker, G.N., Richardson, J.D., and Eiges, P.E.: 2005b, Sharp boundaries of small- and middle-scale solar wind structures, *J. Geophys. Res.* **110**, A12110.
- Riazantseva, M.O., Khabarova, O.V., Zastenker, G.N., and Richardson, J.D.: 2007, Sharp boundaries of the solar wind plasma structures and their relationship to the solar wind turbulence. *Adv. Space Res.* **40**, 1802-1806.
- Roberts, D. A., Keiter P.A., and Goldstein M.L.: 2005, Origin and dynamics of the heliospheric streamer belt and current sheet. *J. Geophys. Res.* **110**, A06102.
- Romanova, N., Pilipenko, V., Crosby, N., and Khabarova, O.: 2007, ULF wave index and its possible applications in space physics. *Bulgarian J.Phys.***34**, 136-148 http://www.bjp-bg.com/papers/bjp2007_2_136-148.pdf .
- Safrankova, J., Zastenker, G.N., Nemecek, Z., et al.: 1997, Small scale observations of magnetopause motion: preliminary results of the INTERBALL project, *Ann. Geophys.*, **15**, 562-569.
- Schwenn, R.: 1990, Large-scale structure of the interplanetary medium. Physics of the Inner Heliosphere I, Springer-Verlag, New York, 99– 181.
- Smith, E. J.: 2001, The heliospheric current sheet. *J. Geophys. Res.*, **106**, 15819-15831.
- Steiger, von R., Schwadron, N., Fisk, L., Geiss, J., Gloeckler, G., Hefti, S., et al.: 2000, Composition of quasi-stationary solar wind flows from Ulysses/Solar Wind Ion Composition Spectrometer. *J. Geophys. Res.* **105**, 27217-27238.

- Svalgaard, L.: 1973, Geomagnetic responses to the solar wind and solar activity. NASA SUIPR report no.555, <http://www.leif.org/research/Geomagnetic-Response-to-Solar-Wind.pdf>
- Svalgaard, L.: 1975, On the use of Godhavn H component as an indicator of the interplanetary sector polarity. *J. Geophys. Res.* **80**, 2717-2722.
- Svalgaard, L., Wilcox, J.M., Scherrer P.H., and Howard R.: 1975, The Sun's magnetic sector structure, *Solar Phys.* **45**, 83-91.
- Velli, M. and Grappin, R.: 1993, Properties of the solar wind. *Adv. Space Res.* **13**, 49-58.
- Wang, Y.-M.; Sheeley, N.R.Jr.: 1990, Solar wind speed and coronal flux-tube expansion. *Astrophys. J.* **355**, 726-732.
- Wang, Y.-M.: 1993, Flux-tube divergence, coronal heating, and the solar wind. *Astrophys. J. Letters* 410, L123-L126.
- Watari, S., and Watanabe, T.: 2006, Sector boundary crossings and geomagnetic activities, *Adv. in Geosciences* **2 ST**, 135-142.
- Wilcox, J.M. and Ness, N.F.: 1965, Quasi-stationary corotating structure in the interplanetary medium. *J. Geophys. Res.* **70**, 5793-5805.

Figures

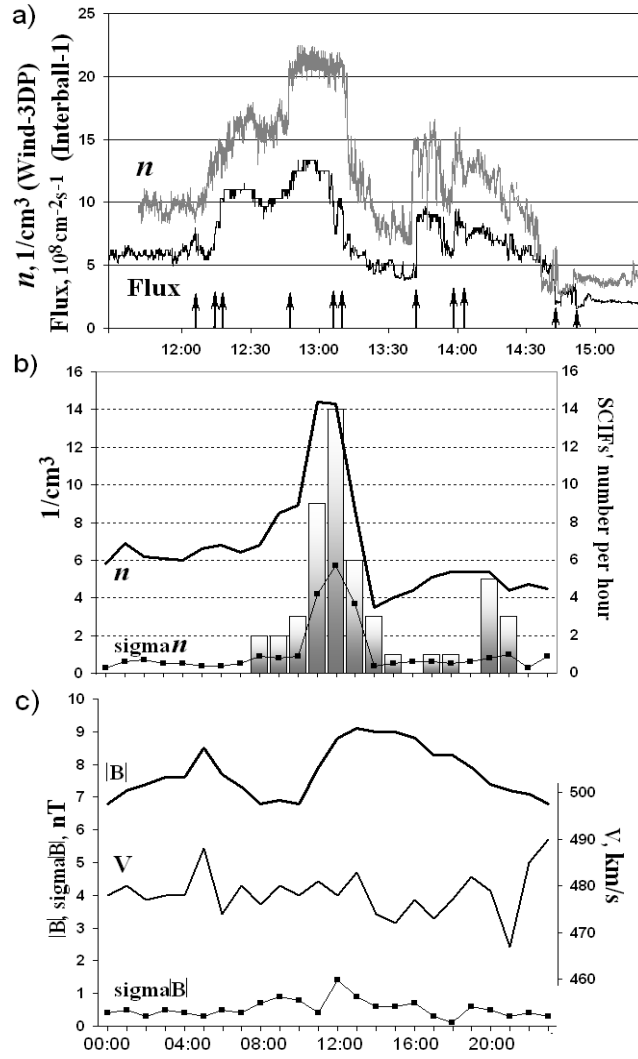


Figure 1 Typical case of the observation of sharp ion flux and density increases/decreases on 26 April 1998. (a) Solar wind density n (WIND) and ion flux \mathbf{Flux} (Interball-1) high-resolution time series. Onsets of SCIFs with amplitude $\geq 2 \times 10^8 \text{ cm}^{-2} \text{ s}^{-1}$ are pointed with arrows in \mathbf{Flux} . (b) Vertical boxes show number of SCIFs with amplitude $\geq 0.5 \times 10^8 \text{ cm}^{-2} \text{ s}^{-1}$ per hour. Time series of 1-h OMNI2 data n , interplanetary magnetic field averaged magnitude $|B|$, solar wind speed V , and standard deviations from mean σn , and $\sigma |B|$ for April 26th, 1998 are given in (b) and (c).

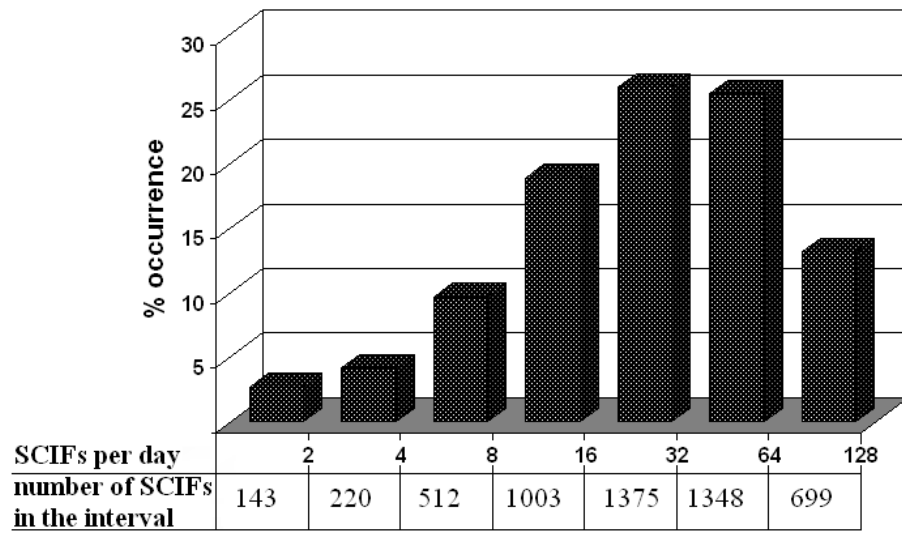


Figure 2 Distribution of 5 300 SCIFs (amplitude $\geq 2 \times 10^8 \text{ cm}^{-2} \text{ s}^{-1}$) as a percentage of the whole number of events for 1996–2000.

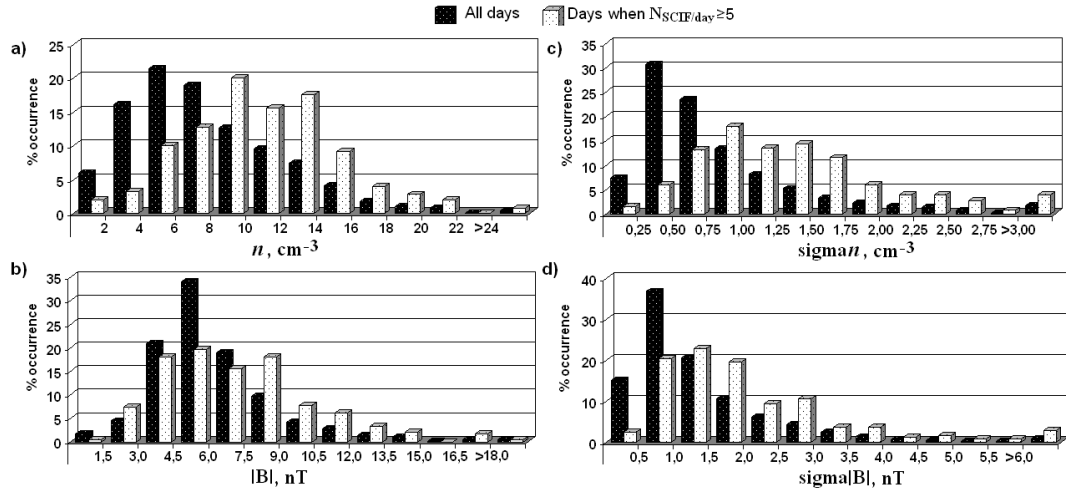


Figure 3. Distribution of daily averaged solar wind parameters: density (a), averaged interplanetary magnetic field magnitude (b), and their standard deviations (c and d) for the days when the number of SCIFs per day exceeded five (white histograms) in comparison with distributions of the same parameters from WIND SWE data (black histograms) for 1996–2000.

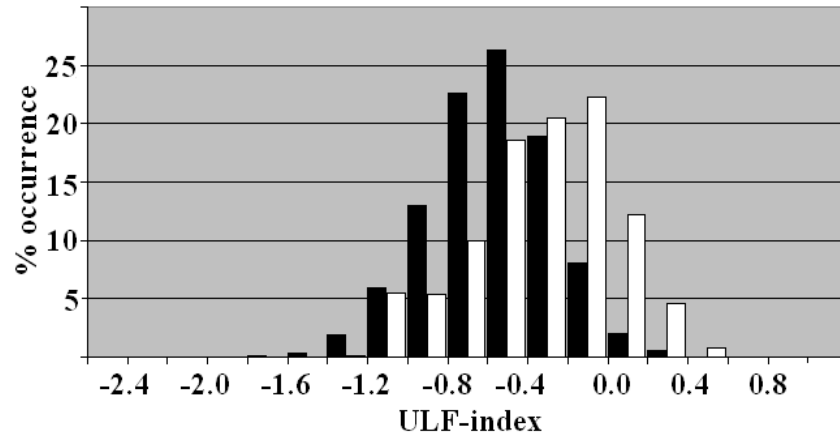


Figure 4 Histograms of distribution of the daily values of the interplanetary ULF-wave index for days of high SCIFs number (white histogram) and for whole period of measurements 1996–2000 (black histogram).

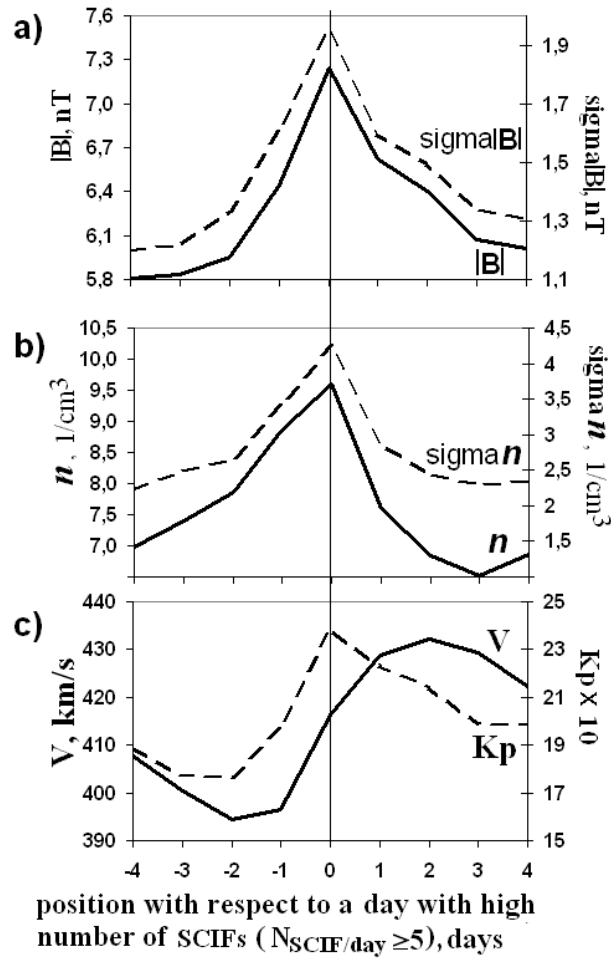


Figure 5 Superposed epoch analysis results for solar wind parameters around the days of high SCIFs' number observation ($N_{\text{SCIF/day}} \geq 5$), 264 events. Daily values of solar wind IMF averaged magnitude $|B|$, density n , speed V , standard deviations $\text{sigma}|B|$, $\text{sigma}n$ and Kp-index of geomagnetic activity are averaged in time vicinity ± 4 days around zero-day.

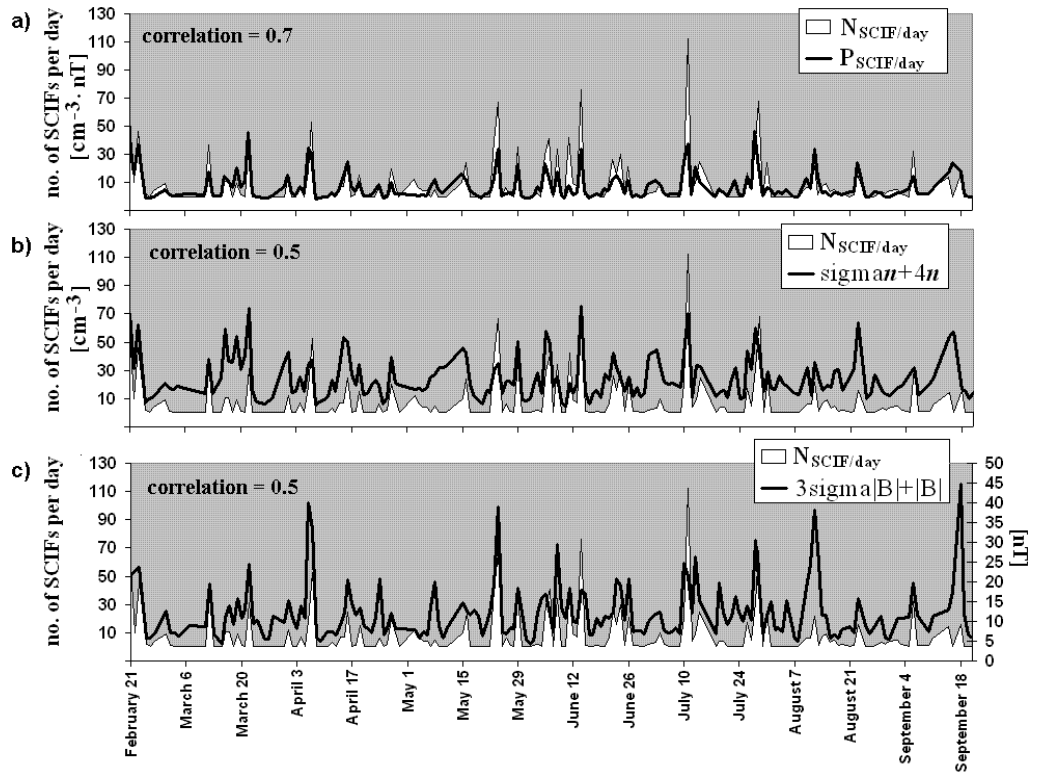


Figure 6 Simulation of SCIFs number per day. $N_{\text{SCIF/day}}$ (white filled curve) is the experimentally observed number of sharp ion flux changes per day by Interball-1 in 2000. (a) $P_{\text{SCIF/day}}$ (black curve) - modelling parameter. (b) and (c) - plasma and IMF multipliers of the modelling parameter $P_{\text{SCIF/day}}$.

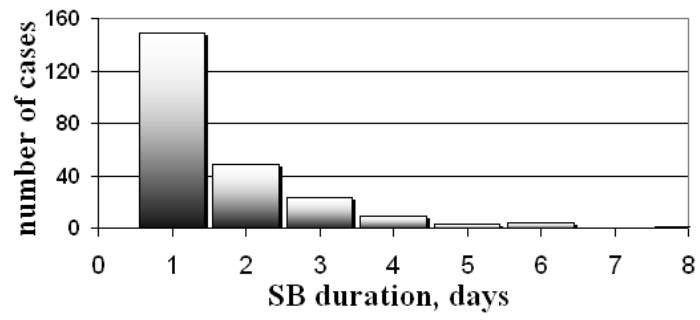


Figure 7 Durations of sector boundary crossings for 1994–2000 according to the ISTP Solar Wind Catalog Candidate Events for 1994–2000

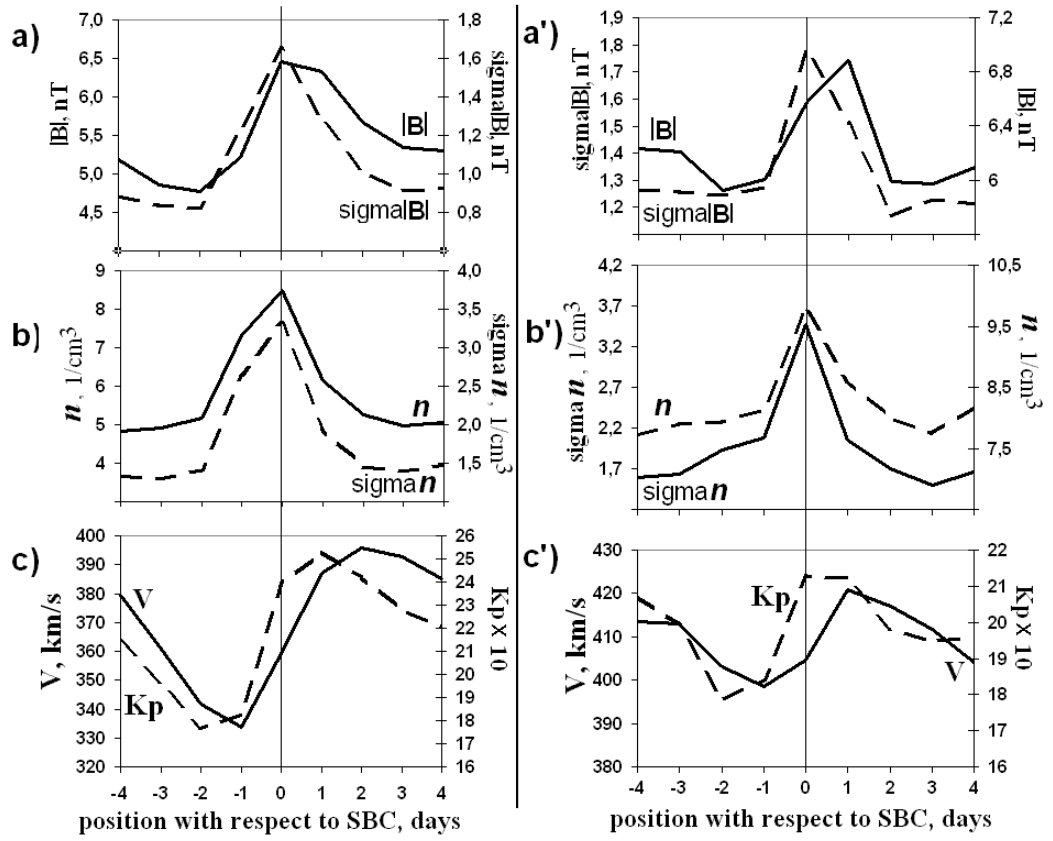


Figure 8 Same as Figure 5, but zero-day corresponds to days of sector boundaries crossing (a–c). Behaviour of parameters for 1300 events from January 1964 to April 2010 from the SBC List by Leif Svalgaard, (a'–c') and for 149 events of one-day sector boundaries crossings from the ISTEP Solar Wind Catalogue of Candidate Events for 1994–2000.

Figure legends

Figure 1 Typical case of the observation of sharp ion flux and density increases/decreases on 26 April 1998. (a) Solar wind density n (WIND) and ion flux **Flux** (Interball-1) high-resolution time series. Onsets of SCIFs with amplitude $\geq 2 \times 10^8 \text{ cm}^{-2} \text{ s}^{-1}$ are pointed with arrows in **Flux**. (b) Vertical boxes show number of SCIFs with amplitude $\geq 0.5 \times 10^8 \text{ cm}^{-2} \text{ s}^{-1}$ per hour. Time series of 1-h OMNI2 data n , interplanetary magnetic field averaged magnitude $|B|$, solar wind speed V , and standard deviations from mean $\text{sigma}n$, and $\text{sigma}|B|$ for April 26th, 1998 are given in (b) and (c).

Figure 2 Distribution of 5 300 SCIFs (amplitude $\geq 2 \times 10^8 \text{ cm}^{-2} \text{ s}^{-1}$) as a percentage of the whole number of events for 1996–2000.

Figure 3. Distribution of daily averaged solar wind parameters: density (a), averaged interplanetary magnetic field magnitude (b), and their standard deviations (c and d) for the days when the number of SCIFs per day exceeded five (white histograms) in comparison with distributions of the same parameters from WIND SWE data (black histograms) for 1996–2000.

Figure 4 Histograms of distribution of the daily values of the interplanetary ULF-wave index for days of high SCIFs number (white histogram) and for whole period of measurements 1996–2000 (black histogram).

Figure 5 Superposed epoch analysis results for solar wind parameters around the days of high SCIFs' number observation ($N_{\text{SCIF/day}} \geq 5$), 264 events. Daily values of solar wind IMF averaged magnitude $|B|$, density n , speed V , standard deviations $\text{sigma}|B|$, $\text{sigma}n$ and Kp-index of geomagnetic activity are averaged in time vicinity ± 4 days around zero-day.

Figure 6 Simulation of SCIFs number per day. $N_{\text{SCIF/day}}$ (white filled curve) is the experimentally observed number of sharp ion flux changes per day by Interball-1 in 2000. (a) $P_{\text{SCIF/day}}$ (black curve) - modelling parameter. (b) and (c) - plasma and IMF multipliers of the modelling parameter $P_{\text{SCIF/day}}$.

Figure 7 Durations of sector boundary crossings for 1994–2000 according to the ISTP Solar Wind Catalog Candidate Events for 1994–2000

Figure 8 Same as Figure 5, but zero-day corresponds to days of sector boundaries crossing (a–c). Behaviour of parameters for 1300 events from January 1964 to April 2010 from the SBC List by Leif Svalgaard, (a'–c') and for 149 events of one-day sector boundaries crossings from the ISTP Solar Wind Catalogue of Candidate Events for 1994–2000.

Tables

Table 1 Mean value, median, standard deviation and skewness for the solar wind parameters in Figure 3.

	Mean	Median	Std.Dev.	Skewness	Valid N
$n_{all} \text{ cm}^{-3}$	7.5	6.6	4.3	1.0	1557
$n_{scif} \text{ , cm}^{-3}$	10.5	10.3	4.4	0.4	250
$\sigma n_{all} \text{ cm}^{-3}$	0.8	0.6	0.7	3.2	1555
$\sigma n_{scif} \text{ , cm}^{-3}$	1.4	1.2	0.9	2.8	250
$ B_{all} \text{ , nT}$	6.0	5.5	2.6	1.7	1546
$ B_{scif} \text{ , nT}$	6.9	6.4	3.2	1.0	245
$\sigma B_{all} \text{ , nT}$	1.3	1.0	1.2	4.2	1546
$\sigma B_{scif} \text{ , nT}$	2.0	1.6	1.4	2.1	245

Table 2 Mean values, 95% confidence interval, and standard deviations in the extreme points for the solar wind parameters and the Kp-index of geomagnetic activity in Figure 5.

	$ B $	$\sigma B $	n	V	σn	K_p
mean	6.23	1.42	7.50	414.4	2.70	20.04
95% confidence interval	0.41	0.18	0.49	10.8	0.37	1.46
standard deviation in the extremum	3.36	1.46	4.10	89.9	3.1	12.10

Table 3 Coefficients of correlation of daily averaged solar wind parameters with SCIF's number per day $N_{SCIF/day}$ (low correlation)

	$N_{SCIF/day}$
V	0.07
σV	0.22
Electric field	0.02
beta	0.05
Mach number	0.05

Table 4 Coefficients of correlation of daily averaged solar wind parameters with SCIF's number per day $N_{SCIF/day}$ (moderate correlation)

	$N_{SCIF/day}$
n	0.5
σn	0.3
$ B $	0.4

$\sigma B $	0.4
$\sigma n + 4n$	0.5
$3\sigma B + B $	0.5

Table 5 Mean values, 95% confidence interval, and standard deviation in the maximum points of the solar wind parameters as well as Kp-index of geomagnetic activity (Figure 8abc)

	$ B $	$\sigma B $	n	V	σn	K_p
mean	5.44	1.05	5.67	373.4	1.76	21.84
95% confidence interval	0.21	0.08	0.34	10.5	0.19	0.64
standard deviation in the maximum	3.93	1.55	6.31	193	3.45	11.8

Table 6 As Table 5, but for Figure 8a'b'c'

	$ B $	$\sigma B $	n	V	σn	K_p
mean	6.25	1.34	7.42	410.0	2.44	19.92
95% confidence interval	0.35	0.19	0.90	13.6	0.59	1.69
standard deviation in the maximum	2.15	1.19	5.63	84.6	3.68	10.51